



## RESEARCH ARTICLE

## Process Systems Engineering

## Integrated metal-organic framework (MOF) and pressure/vacuum swing adsorption process design: MOF matching

Xiang Zhang<sup>1</sup> | Teng Zhou<sup>1,2</sup>  | Kai Sundmacher<sup>1,2</sup> <sup>1</sup>Department for Process Systems Engineering, Max Planck Institute for Dynamics of Complex Technical Systems, Magdeburg, Germany<sup>2</sup>Chair of Process Systems Engineering, Otto-von-Guericke University Magdeburg, Magdeburg, Germany

## Correspondence

Teng Zhou, Department for Process Systems Engineering, Max Planck Institute for Dynamics of Complex Technical Systems, Sandtorstr. 1, Magdeburg D-39106, Germany. Email: [zhout@mpi-magdeburg.mpg.de](mailto:zhout@mpi-magdeburg.mpg.de)

## Funding information

European Regional Development Fund, Grant/Award Number: Research Center of Dynamic Systems; Max-Planck-Gesellschaft, Grant/Award Numbers: Ernst Dieter Gilles Postdoctoral Fellowship, Junior Professorship of OvGU Magdeburg

## Abstract

A two-step integrated metal-organic framework (MOF) and pressure/vacuum swing adsorption (P/VSA) process design has been recently established for gas separation. In the first step, selected MOF descriptors and process operating conditions are simultaneously optimized to maximize the process performance. Based on the obtained results, the second step (i.e., MOF matching) is addressed and exemplified by propene/propane separation in this work. Computational MOF synthesis and screening are explicitly carried out to find new advanced material candidates for enhancing the separation process efficiency. First, model-based property-performance relationships are developed for fast MOF screening. Then, MOF building blocks are extracted from 471 MOFs contained in the Computation-Ready Experimental (CoRE) MOF database. With these building blocks, 45,472 hypothetical MOFs are created. After model-based and molecular simulation-based screening, six candidates are left and sent to P/VSA process optimization. Finally, three candidates are found to meet the predefined separation specifications and one candidate shows a better process performance than the best out of the 471 CoRE MOFs.

## KEYWORDS

descriptors, integrated material and process design, metal organic frameworks, MOF screening, pressure/vacuum swing adsorption, propene/propane separation

## 1 | INTRODUCTION

Pressure/vacuum swing adsorption (P/VSA) has been widely used in the chemical and energy industries for gas separation. In P/VSA processes, gases are separated based on their different affinities on solid adsorbents at different pressures. So far, extensive research works have been done on adsorbent selection and P/VSA process optimization. For adsorbent selection, various computational screening methods have been developed to identify suitable candidates such as metal-organic frameworks (MOFs) and zeolites for different applications.<sup>1–5</sup> In general, a set of adsorbents are collected and their adsorption and diffusion properties are calculated using molecular

simulations. Then, simple performance metrics are calculated to identify promising candidates. On the other hand, P/VSA processes are modeled with complicated partial differential equations and a number of model reduction and substitution techniques as well as advanced algorithms have been proposed for efficiently optimizing P/VSA processes.<sup>6–8</sup> Despite many progress in these two areas, it is worth noting that to select adsorbents and optimize P/VSA processes separately is insufficient to obtain a truly optimal P/VSA process. It has been widely recognized that P/VSA process design is a multi-scale design problem that incorporates inter-linked adsorbent material, gas-solid phase, and P/VSA process levels.<sup>9–11</sup> Variations of adsorbent materials and process operating conditions can simultaneously

This is an open access article under the terms of the [Creative Commons Attribution-NonCommercial](https://creativecommons.org/licenses/by-nc/4.0/) License, which permits use, distribution and reproduction in any medium, provided the original work is properly cited and is not used for commercial purposes.

© 2022 The Authors. *AIChE Journal* published by Wiley Periodicals LLC on behalf of American Institute of Chemical Engineers.

affect the adsorption behavior in the gas–solid phase and hence jointly determine the final process performance. Therefore, integrated adsorbent and P/VSA process design is highly desired to find high-performance adsorbents that serve the process best.

Typically, an integrated material and process design task can be formulated as an optimization problem. Different mathematical models are used to represent different levels, which enables the optimization of design variables at different levels simultaneously. For adsorption processes, Khurana and Farooq<sup>12,13</sup> simultaneously optimized predefined isotherm characteristics and VSA process operating conditions for carbon capture. Optimal isotherm shapes achieving the best capture performance are obtained to serve as targets for adsorbent design. However, it is still unknown whether a specific adsorbent can match the isotherm targets. There is always a danger that the isotherm targets cannot be satisfied by any adsorbent materials in the world. Considering this issue, adsorbent material design should be explicitly studied to completely solve the multi-scale P/VSA design problem. In this way, the chemistry and structure of feasible adsorbent materials whose isotherms are close to the desired targets can be identified. Currently, most adsorbents have been synthesized using the experimental trial-and-error approach that is time-consuming and inefficient. Importantly, it is difficult to find novel adsorbents with desired isotherm properties. Alternatively, computational synthesis approaches can explore a large design space and efficiently generate new promising candidates to guide material scientists for experimental validation.<sup>14,15</sup>

So far, much progress has been achieved on computational synthesis and screening of adsorbents (e.g., MOFs and covalent-organic frameworks) for gas storage<sup>16–19</sup> and separation.<sup>20–23</sup> In general, a large number of hypothetical MOFs are first created using different tools and their adsorption isotherms for target species are predicted via molecular simulations or tailor-made models. Then, promising candidates are ranked with respect to desired storage (e.g., large delivery capacity) or separation (e.g., large adsorption capacity and selectivity) performance metrics at prespecified conditions (e.g., temperature, pressure, and gas compositions). For instance, Lee et al.<sup>18</sup> used *pormake* to construct hypothetical MOFs. Machine learning models

are trained for isotherms prediction and the MOFs with highest methane delivery capacity were identified by evolutionary-based optimization. In addition, Yao et al.<sup>20</sup> developed a new machine learning-based platform to design MOFs for carbon capture. As represented by a vector of building block symbols, new MOFs are computationally generated and screened based on their CO<sub>2</sub> adsorption capacity and selectivity that are calculated in fixed adsorption conditions. It is noted that for gas storage, the adsorption and desorption conditions are usually predefined and widely agreed. In this case, the use of simple performance metrics for adsorbent screening can rank potential candidates reasonably. However, for gas separation, the process configuration and operating conditions can vary significantly. Due to this reason, simple performance metrics can neither tell whether specific separation requirements are achieved with an adsorbent nor rank the adsorbents correctly in terms of process performance.<sup>24–26</sup> To fill this gap, the insights drawn from phase and process levels should be inserted into the procedures of adsorbent synthesis and screening. Combined with process optimization and evaluation, optimal MOFs with a real best process performance can be successfully identified.

Following the above strategy, the authors' group recently proposed a two-step integrated MOF and P/VSA process design methodology (see Figure 1) to solve the multi-scale design problem. In the first article of this series, Step 1 (i.e., descriptor optimization) has been elaborated and published.<sup>11</sup> Only optimal MOF descriptors have been obtained, instead of any hypothesized MOFs with known topology and chemistry. As a continuous effort, this work presents the subsequent step: MOF matching. The aim is to computationally synthesize and screen hypothetical MOFs for enhancing equilibrium-based propene/propane (PE/PA) separation. The design guidelines and data-driven models obtained from Step 1 are well adopted in the present work for designing new MOFs that can eventually result in better separation performance using optimized P/VSA processes. The rest of this article is organized as follows. First, a brief overview of Step 1 is provided. Then, detailed property-performance relationships are developed for fast preliminary MOF screening. Finally, MOF building blocks are specified to perform *in silico* MOF design and the optimal hypothetical MOF is discussed.

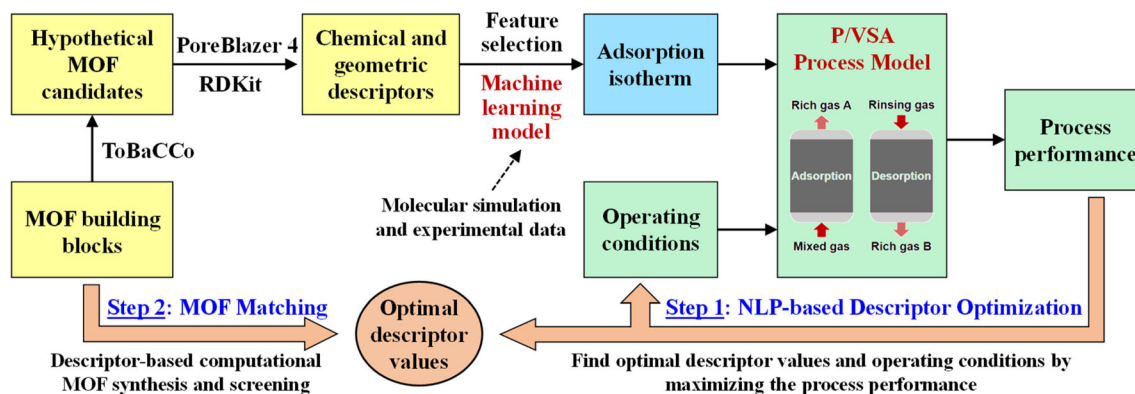


**FIGURE 1** General methodology for integrated metal-organic framework and pressure/vacuum swing adsorption process design

## 2 | REVIEW OF STEP 1: DESCRIPTOR OPTIMIZATION

The workflow of Step 1 is shown in the right side of Figure 1. MOFs are first represented as a set of 5009 chemical and 14 geometric descriptors. Four hundred seventy one MOFs contained in the Computation-Ready Experimental (CoRE) MOF database with considerable diversity are selected and their descriptors are calculated accordingly. In addition, the single-component adsorption isotherms of PE and PA on these 471 MOFs at 300 K are collected.<sup>27</sup> Based on the calculated descriptors and collected isotherm data, 19 most influential descriptors are selected and treated as design variables representing MOF variations, including

- 9 geometric descriptors: bulk density, pore limiting diameter, largest cavity diameter, volumetric surface area, void fraction, unit length  $a$ , unit length  $b$ , unit length  $c$ , volume per unit cell
- 10 chemical descriptors: number of atoms, non-H atoms, metal atoms, transition metal atoms, double bonds, ring bonds, bond to metal atoms, and alkyl groups as well as frequency of C–N at topological distance 1 and C–O at topological distance 2

Using the above 19 descriptors as input, two artificial neural network (ANN) models predicting single-component adsorption loadings of PE and PA were trained and further used to derive multi-component dual-site Langmuir (DSL) isotherm models that can provide accurate mixture adsorption equilibrium predictions for the PE/PA system. In addition, a support vector machine (SVM) based classifier model was developed to define the valid design space of the 19 descriptors. Finally, the design space, isotherms, and one-bed four-step isothermal P/VSA process models were combined together. Under specific separation requirements, that is, to produce 99% PE with no less than 30% recovery from a two-atmospheric 85%/15% PE/PA mixture, integrated MOF and P/VSA process design problem was explicitly formulated as a nonlinear programming (NLP) problem. Given prespecified input parameters (i.e., gas properties, equipment specifications, etc. listed in Supporting Information), the 19 MOF descriptors and 6 process operating conditions (i.e., adsorption and desorption pressures as well as the durations of four steps) were optimized simultaneously to minimize the total energy consumption. As a result, the optimal descriptor values, adsorption isotherms, and P/VSA operating conditions were obtained. These information will be utilized for computational MOF design in this work.

## 3 | PROPERTY-PERFORMANCE RELATIONSHIPS FOR EFFICIENT MOF SCREENING

Reliable material-property-performance relationships are crucial for solving the multi-scale design problem. For MOF-based equilibrium separation, the thermodynamic properties of MOFs (i.e., adsorption

isotherms) have dominant impact on the process performance. As stated above, two ANN models have been trained in Step 1 to predict single-component adsorption uptakes of PE and PA from 19 MOF descriptors. This can serve as material-property relationships. The next task is to build model-based property-performance relationships. These mathematical relationships allow for a fast and preliminary screening of MOFs, which prevents the conduction of process optimization for every MOF candidate. Here, proper property-performance relationships are first developed on the basis of the optimal isotherms obtained from Step 1. Their reliability is further verified with the 471 MOFs.

### 3.1 | Property-performance relationship for PE/PA separation

Referring to the method proposed by Iyer and Hasan,<sup>28</sup> property-performance relationships of adsorbent materials are constructed by sampling various adsorption isotherms followed by process optimizations. By doing so, the obtained results can reveal the inherent correlations between adsorption equilibrium and process feasibility. To be consistent with Step 1, the single-component DSL isotherm model in Equation 1 and its binary extensions in Equation 2 are used to represent single-component and multi-component adsorption equilibria, respectively.

$$q^{\text{eq}} = \frac{Q^1 \cdot b^1 \cdot P}{(1 + b^1 \cdot P)} + \frac{Q^2 \cdot b^2 \cdot P}{(1 + b^2 \cdot P)} \quad (1)$$

$$q_E^{\text{eq}} = \frac{Q_E^1 \cdot b_E^1 \cdot P \cdot y_E}{1 + b_E^1 \cdot P \cdot y_E + b_A^1 \cdot P \cdot y_A} + \frac{Q_E^2 \cdot b_E^2 \cdot P \cdot y_E}{1 + b_E^2 \cdot P \cdot y_E + b_A^2 \cdot P \cdot y_A} \quad (2a)$$

$$q_A^{\text{eq}} = \frac{Q_A^1 \cdot b_A^1 \cdot P \cdot y_A}{1 + b_E^1 \cdot P \cdot y_E + b_A^1 \cdot P \cdot y_A} + \frac{Q_A^2 \cdot b_A^2 \cdot P \cdot y_A}{1 + b_E^2 \cdot P \cdot y_E + b_A^2 \cdot P \cdot y_A} \quad (2b)$$

where the subscripts  $E$  and  $A$  denote PE and PA, respectively.  $q^{\text{eq}}$  is the adsorption equilibrium loading at pressure  $P$ .  $y$  is the molar fraction in the gas phase.  $Q$  and  $b$  are DSL model parameters. With the DSL models, the thermodynamic properties of any MOF can be characterized by the eight model parameters (i.e.,  $Q_E^1$ ,  $b_E^1$ ,  $Q_E^2$ ,  $b_E^2$ ,  $Q_A^1$ ,  $b_A^1$ ,  $Q_A^2$ , and  $b_A^2$ ). From the process perspective, the eight parameters directly determine the adsorption process performance. In this situation, different combinations of the eight parameters were sampled and then used for rigorous P/VSA process optimization. Note that all the model parameters refer to a fixed temperature of 300 K, since only an isothermal P/VSA process at 300 K is focused in this series. Here, the Latin Hypercube sampling approach was used to generate samples randomly and uniformly. Additional constraints were added to ensure that the samples were distributed around the optimal isotherms obtained in Step 1. This avoids redundant isotherm samples and reduce unnecessary process optimizations. The detailed constraints are given below.

- In the optimal isotherms, the PE and PA adsorption loadings at 2 atm are 3.7 and 1.4 mol/kg, respectively. Thus, the saturated adsorption capacities  $Q_E^1$  and  $Q_E^2$  were sampled within 0.01–6 mol/kg while  $Q_A^1$  and  $Q_A^2$  were varied within 0.01–4 mol/kg. The affinity parameters  $b_E^1$ ,  $b_E^2$ ,  $b_A^1$ , and  $b_A^2$  were allowed to vary between 0.01 and 20 (1/bar). In addition, the samples whose PE and PA adsorption loadings at 2 atm exceed 5 and 2.5 mol/kg, respectively, were discarded.
- Since only PE-selective MOFs are studied, the adsorption capacity on PE should be larger than that on PA when pressure exceeds 0.1 atm.
- Considering the separation specifications (i.e., 99% PE purity with no less than 30% recovery), the isotherm samples were discarded when the difference of the associated PE and PA adsorption loadings at 2 atm is less than 0.5 mol/kg.

Considering the computational burdens of complex P/VSA process optimization, 400 samples were generated. Figure S1 shows the single-component isotherms of PE and PA for all the 400 samples. It can be seen that the samples span adequate isotherm spaces and are well distributed around the optimal isotherms highlighted. These isotherm samples were directly used for P/VSA process optimization. The P/VSA process configuration and models used here are exactly the same as those employed in Step 1. The process is presumably operated in one bed at 300 K. A complete process cycle consists of pressurization, adsorption, rinsing, and desorption steps. The resulting optimization problem is summarized in Equation 3. As indicated, the total energy consumption per ton of purified PE product is minimized by optimizing six design variables, namely adsorption ( $P_{AD}$ ) and desorption ( $P_{DE}$ ) pressures as well as the durations of the four steps ( $t_{PR}$ ,  $t_{AD}$ ,  $t_{RI}$ , and  $t_{DE}$ ). The constraints include mass balances, mass transfer kinetics, DSL isotherm models, pressure drop correlation, cyclic steady state, boundary conditions, as well as purity ( $\xi_E$ ) and recovery ( $\theta_E$ ) specifications. For concision, the detailed model equations and descriptions are not repeated here. They can be found in our first article.<sup>11</sup>

$$\min E(P_{AD}, P_{DE}, t_{PR}, t_{AD}, t_{RI}, t_{DE}) \quad (3)$$

$s.t. \frac{\partial y_i}{\partial t} = f_1(y_i, u, P, q_E, q_A)$	gas–phase component mass balances
$\frac{\partial P}{\partial t} = f_2(P, u, q_E, q_A)$	total mass balance
$\frac{\partial q_i}{\partial t} = f_3(q_i^{eq}, q_i)$	solid–phase balances and mass transfer kinetics
$f_4(q_i^{eq}, P, y_i) = 0$	DSL isotherm models
$f_5(P, u, y_A, y_E) = 0$	pressure drop
$f_6(y_i, q_i, P, u) = 0$	cyclic steady state and boundary conditions
$f_7(\xi_E, t_{DE}, u, P, y_E) = 0$	purity specification
$f_8(\theta_E, t_{PR}, t_{AD}, t_{RI}, t_{DE}, u, P, y_E) = 0$	recovery specification

In total, 400 NLP optimization problems were solved. For easy reference, all the sampled DSL model parameters and the corresponding optimization results are summarized in Supporting

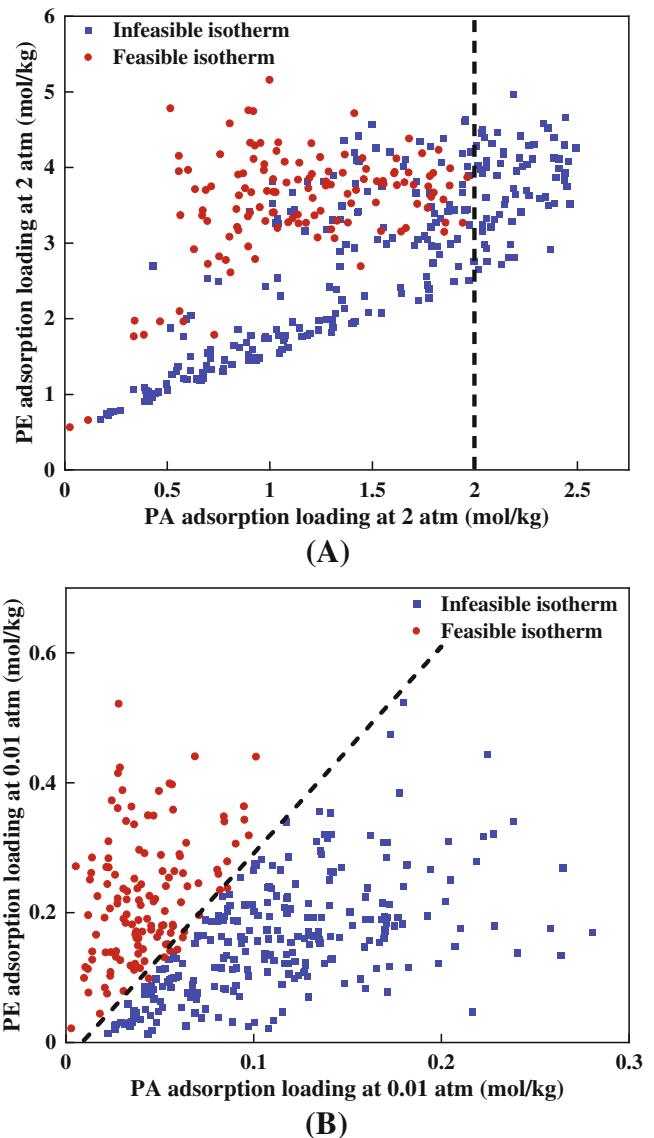


**FIGURE 2** Feasibility maps based on (A) adsorption loadings at 2 atm and (B) adsorption loadings at 0.01 atm for deriving property-performance relationships

Information. It is obvious that not all the isotherms can satisfy the separation specifications. After careful analysis of the optimization results, two feasibility maps were obtained and shown in Figure 2. Figure 2A shows the feasible regions with respect to the single-component adsorption loadings at 2 atm. It is observed that within the sampled isotherm space, when the PA adsorption loading at 2 atm ( $q_A^2$ ) exceeds 2 mol/kg, the isotherm samples cannot meet the separation requirements. Therefore, as written in Equation 4,  $q_A^2$  is expected to be less than 2 mol/kg for feasible PE/PA separation.

$$q_A^2 \leq 2 \quad (4)$$

Figure 2B shows the feasible map with respect to adsorption uptakes at 0.01 atm ( $q^{0.01}$ ) that are representative of the initial

isotherm slopes (i.e., Henry constant). The samples can be roughly divided into feasible and infeasible regions. After a linear classification performed using the scikit-learn package in Python 3, a linear classifier model (see black dot line) was obtained to separate the whole region into two. With the extracted slope and intercept, the constraint in Equation 5 must be satisfied to ensure that a sample is located in the feasible region.

$$q_E^{0.01} \geq 3.185 \times q_A^{0.01} - 0.027 \quad (5)$$

Clearly, the above two constraints represent the quantitative correlations between adsorption properties and process feasibility. Notably, the single-component PE and PA adsorption loadings at 300 K can be directly predicted with the 19 MOF descriptors and pressure using the established ANN models.

### 3.2 | Validation with 471 CoRE MOFs

To further validate the reliability of the above two constraints, the process feasibility of the 471 CoRE MOFs were investigated. The collected adsorption loadings of the 471 CoRE MOFs were used to fit the single-component DSL isotherm models. The fitting was performed using the *lmfit* package and the Levenberg–Marquardt algorithm in Python 3.8. After model fitting, the resulting DSL models were used to predict the adsorption uptakes of PE and PA at 0.01 and 2 atm. For simplicity, the fitted DSL model parameters and the predicted adsorption loadings are tabulated in Supporting Information. Based on the predicted loadings, the 471 CoRE MOFs were verified against the two feasibility constraints. It can be found that 87 CoRE MOFs satisfy the first constraint (Equation 4) and 17 CoRE MOFs meet the second constraint (Equation 5). As a result, Table 1 lists the 15 CoRE MOFs that meet the two constraints simultaneously.

Moreover, P/VSA process optimization was performed for the 471 CoRE MOFs, which provides the true process performance for these MOFs. To do so, the multi-component DSL isotherm models in the form of Equation (2) were derived based on the fitted single-component DSL model parameters and directly imported into the P/VSA process model for optimization. As listed in Tables 1, 9 CoRE MOFs can meet the required PE/PA separation specifications. It can be seen that 8 out of the 9 CoRE MOFs meet the two feasibility constraints except *FIQCEN* (i.e., Cu-BTC or HKUST-1). This is because its PA adsorption uptake at 2 atm is 7.76 mol/kg, which is unable to satisfy the first feasibility constraint. In summary, the results demonstrate that the two constraints can effectively filter out MOFs that are infeasible to achieve the prespecified separation requirements. In addition, the best of the 471 CoRE MOFs is *SEYDUW* that refers to ( $\mu$ 3-N-[phosphonomethyl]iminodiacetato)-diaqua-yttrium-mono-hydrate.<sup>29</sup> The corresponding minimum energy consumption is 91.99 kWh/ton PE. This can act as a new benchmark for the subsequent computational MOF design.

**TABLE 1** Results of the screening of 471 CoRE MOFs using the two property-performance relationship constraints

CoRE MOFs fulfilling the two feasibility constraints	
BERFIP, FAQVEA, MIDRAT, OSAXAI, QUJFUX, QUVDUH, SEYDUW, SUJQOE, VASKOR, VISTUM, WABTOK, WIDZOA, XEHTUB, XOVVIO, XUYYAR	
CoRE MOF	Energy consumption (kWh/ton PE)
SEYDUW	91.99
QUJFUX	97.95
XOVVIO	213.88
VISTUM	250.84
XEHTUB	257.45
FAQVEA	321.40
FIQCEN	505.02
QUVDUH	590.99
SUJQOE	649.17

## 4 | COMPUTATIONAL MOF SYNTHESIS AND SCREENING

As the core of Step 2, new MOFs were computationally designed for efficient PE/PA separation. To do so, proper MOF building blocks were first identified. Then, hypothetical MOFs were synthesized and *in silico* screened to identify top candidates leading to better PE/PA separation performance.

### 4.1 | Identification of MOF building blocks

In general, a MOF consists of metal nodes, organic nodes (if applicable), and organic linkers assembled in a certain topology. For MOFs, at least one type of metal node must exist and some topologies need to be constructed with more than one type of organic node. Moreover, different types of metal/organic node have different coordination numbers that determine the number of organic linkers connected to it. Due to the complex structures of MOFs, there can be multiple ways to dissect MOFs into different building blocks.<sup>30</sup> Referring to the basic rules of constructing hypothetical MOFs, Figure 3 shows a general procedure of extracting MOF building blocks that can be subsequently used for *in silico* MOF synthesis. For a MOF in the form of Crystallographic Information Framework (.cif) file, the open-source program *ToposPro* can be utilized to analyze its topology, and its metal nodes and organic nodes (if applicable) can be identified as well. Afterward, MOFs can be viewed in Material Studio. In doing so, the organic linkers connecting two nodes (mainly metal node–metal node and metal node–organic node) can be identified. Meanwhile, the nodes and linkers can be manually extracted after deleting all the other atoms in the MOF using Material Studio. The extracted nodes and linkers can be subsequently used as building blocks for computational MOF synthesis. Following the above procedures, the topology,

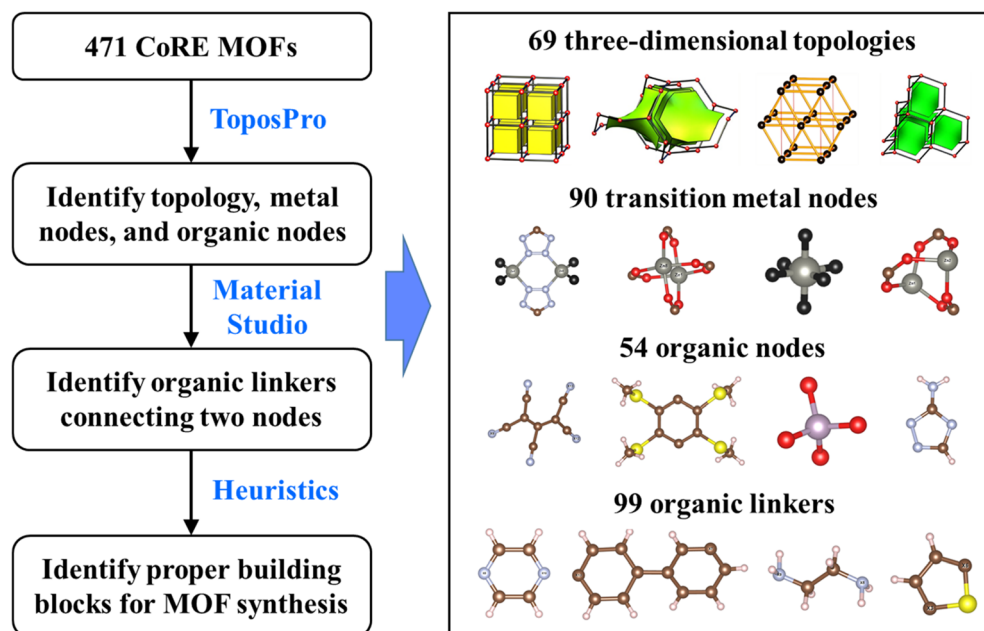


**FIGURE 3** Generation of metal-organic framework (MOF) building blocks from the 471 CoRE MOFs

nodes, and organic linkers of the 471 CoRE MOFs were analyzed, identified, and extracted. The detailed structural decompositions are summarized in Supporting Information. Notably, the following heuristics were considered to discard unusable building blocks.

- The Reticular Chemistry Structure Resource (RCSR) database collected over 2300 different MOF topologies. Each topology is named as a three-letter symbol with or without an extension (i.e., *pqr*-*a* and *pqr*). In addition, the detailed information on each topology (e.g., spatial structure and required types of connecting nodes) has been well documented. In this work, only the extracted topologies that are included in the RCSR database were considered for MOF synthesis, since only the topological templates of these topologies are available in the state-of-the-art MOF synthesis tool.<sup>30</sup>
- Two-dimensional topologies were discarded due to their scarcity.
- The organic linkers and nodes that form over two connections or double/triple bonds with a single metal/organic node were removed, since linkers and nodes as well as nodes and nodes are only allowed to form a single-bond connection in the state-of-the-art MOF synthesis tool.<sup>30</sup>
- The organic nodes with one atom connecting to two different metal nodes were discarded, since such nodes usually lead to infeasible MOFs.
- Asymmetric metal nodes with over 25 atoms were discarded since those metal nodes rarely exist in MOFs.

Regarding the PE/PA separation example, the design guidelines obtained from Step 1 were taken into account as well. They are:

- Only the metal nodes with transition metals were kept. This is because transition metals are expected to introduce open metal

site and  $\pi$ -complexation, which can result in stronger interactions with PE over PA.

- The organic nodes and linkers containing C—O pairs at topological distance 2 (i.e., C—X—O chains) were removed.
- Only the organic nodes and linkers consisting of rings, double bonds, or C—N bonds were retained.

Accordingly, in total 69 three-dimensional topologies, 90 transition metal nodes, 54 organic nodes, and 99 organic linkers were obtained from the 471 CoRE MOFs (Figure 3). For the 69 topologies, their three-letter symbols and the required types of linking nodes are listed in Table S1. The atomic structures of the metal nodes, organic nodes, and organic linkers are given in Tables S2–S4. In addition, the corresponding “cif” files have been uploaded to the Github folder (<https://github.com/zx2012flying/Integrated-MOF-and-PVSA-Process-Design>).

## 4.2 | Computational MOF design

The large number of building blocks obtained above provide a huge design space. Due to the limited computational resources, only the 27 topologies requiring one type of node (i.e., metal node) were adopted. In other words, none of the organic nodes were considered for MOF synthesis. Table 2 lists the three-letter symbols of the 27 topologies and the coordination of the required metal node (i.e., number of free connections). Given this simplification, Figure 4 shows the workflow for the computational MOF synthesis and screening. First, using the finalized building blocks, hypothetical MOFs were generated and their descriptors were calculated. Then, model-based screening was performed to identify promising MOFs. Their feasibilities were further assessed using rigorous GCMC simulations. Finally, P/VSA process

**TABLE 2** Twenty-seven topologies considered for computational metal-organic framework (MOF) design in the PE/PA separation example

Topology	Coordination of metal node	Topology	Coordination of metal node
srs	3	uni	4
ths	3	uog	4
atn	4	usf	4
cag	4	bnn	5
cds	4	sqp	5
dft	4	acs	6
dia	4	lcy	6
dmp	4	pcu	6
lon	4	rob	6
lvt	4	sol	6
qtz	4	sxb	6
sod	4	bcu	8
sra	4	hex	8
unc	4		

optimization was performed to identify the real optimal MOFs. The detailed procedures and models are elaborated below.

#### 4.2.1 | *In silico* synthesis of hypothetical MOFs

The state-of-the-art constructor *ToBaCCo* 3 was employed for *in silico* MOF synthesis. Hypothetical MOFs were constructed on the basis of topological templates that guide the placement of metal nodes and organic linkers. Each topological template consists of the information on the number, coordination, and symmetry of the metal nodes. For the 27 topologies, the coordination of required metal node is given in Table 2. Node symmetry denotes the spatial arrangement of connected organic linkers. During construction, the coordination compatibility between topology and metal node is tested. A topology is regarded as incompatible with a metal node, when the node coordination required for the topology is different from that of the metal node. For the 90 metal nodes, their node coordinations are provided in Table S2. As shown, there are 10 three-coordinated nodes, 37 four-coordinated nodes, 6 five-coordinated nodes, 25 six-coordinated nodes, 11 eight-coordinated nodes, and one 12-coordinated node. In addition, based on the domain knowledge of MOF chemistry, some other factors (e.g., node symmetry, bond connectivity, etc.) are also checked to ensure that only sound feasible MOFs are created. The detailed algorithms in *ToBaCCo* can be found in previous publications.<sup>30,31</sup> In this work, the 90 metal nodes and 99 organic linkers in the form of *cif* files were imported into the *nodes* and *edges* folders in *ToBaCCo*, respectively. For the 27 topologies, their topological templates can be found in the *ToBaCCo* template database. With these information, the differential evolution algorithm implemented in *ToBaCCo* was used for structural scaling. As a result, 45,472 hypothetical MOFs were generated and stored in the form of *cif* files, as shown in Figure 5.

Given the 45,472 hypothetical MOFs, the candidates leading to the best process performance should be identified. For this,

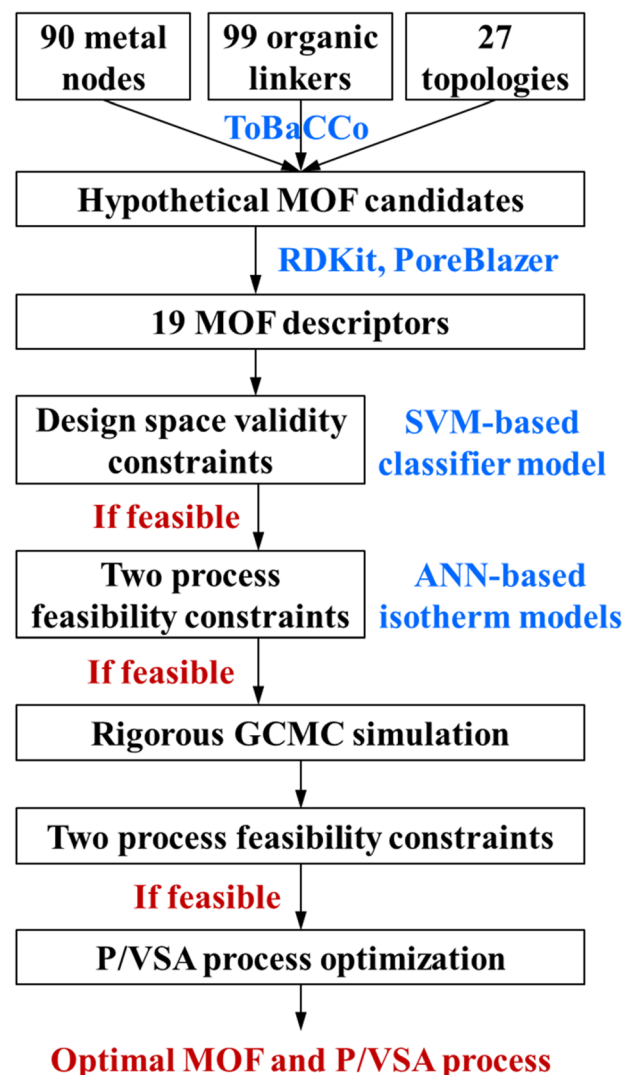


**FIGURE 4** Workflow of the computational metal-organic framework (MOF) synthesis and screening for PE/PA separation

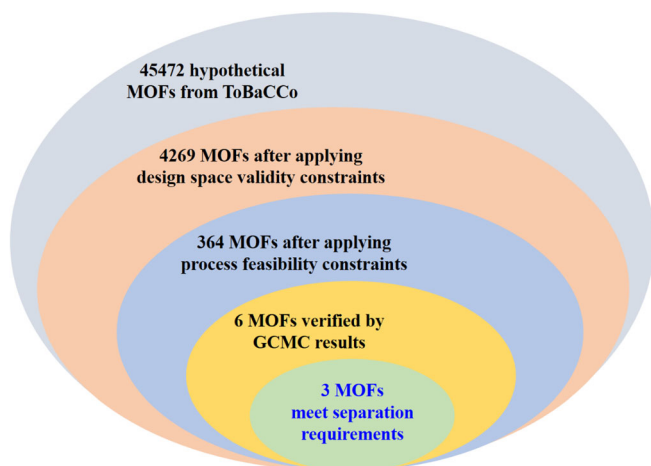


**FIGURE 5** Statistics of screened hypothetical metal-organic framework (MOF) candidates

calculating adsorption isotherms is a prerequisite. Obviously, it is quite computational demanding to perform rigorous GCMC simulations for all the MOF candidates. Alternatively, the ANN-based isotherm models obtained in Step 1 can be applied for an efficient model-based screening where only the 19 descriptors need to be calculated in advance. To do so, the open-source toolbox *OpenBabel* was used to convert the original MOF *cif* files into molfiles (.mol) and XYZfiles (.xyz).<sup>32</sup> The molfiles were directly analyzed using the cheminformatics package *RDKit* to get the detailed information of atoms, bonds, and groups. Accordingly, the 10 chemical descriptors can be calculated based on their definitions given in Step 1.<sup>11</sup> Additionally, different from Step 1 where *Zeo++* was used, the XYZfiles and the *PoreBlazer 4* program were applied for computing geometric descriptors. This is because *PoreBlazer 4* is favored in Python 3 for parallel computing and with the same parameter settings the geometric descriptors from *PoreBlazer 4* and *Zeo++* are almost consistent.<sup>33</sup> Depending on the topology, the computed geometric descriptors were finally scaled to a primitive cell level. Due to the large number of hypothetical MOFs synthesized, descriptor computation was carried out using the parallel computing cluster in our institute that comprises 122 CPU nodes. On average, it takes around 5 minutes for a single CPU node to compute the 19 descriptors for a single MOF. The descriptors of the 45,472 hypothetical MOFs have been uploaded to the Github folder.

#### 4.2.2 | MOF screening via validity and feasibility constraints

Model-based MOF screening was performed using the developed material-property-performance relationships. The idea is to predict adsorption loadings from MOF descriptors using the ANN-based isotherm models. This enables a fast verification of the feasibility constraints in Equations (4) and (5). The detailed screening process is described below.

First, the values of the 19 descriptors were sent to verify whether they were in the validity domain of the ANN-based models. This improves the screening reliability due to the limited extrapolation power of data-driven models. As consistent as Step 1, the constraints on the lower and upper bounds (Equation 6) and the one-class SVM classifier model (Equation 7) are considered here.

$$\mathbf{y}^L \leq \mathbf{y} \leq \mathbf{y}^U \quad \mathbf{y} = [y_1, \dots, y_{19}] \quad (6)$$

$$f(\mathbf{y}) = \sum_{j=1}^2 w_j \cdot \phi_j(\mathbf{y}) + \rho > 0 \quad \mathbf{y} = [y_1, \dots, y_{19}] \quad (7a)$$

$$\phi_j(\mathbf{y}) = e^{-\beta \cdot \|\mathbf{y} - \mathbf{SV}_j\|^2} \quad \mathbf{SV}_j = [SV_{1j}, \dots, SV_{19j}] \quad (7b)$$

where  $\mathbf{y}$  denotes the descriptor vector.  $\mathbf{y}^L$  and  $\mathbf{y}^U$  are the lower and upper bounds, respectively. The bounds were set as the minimal and maximal descriptor values of the 471 CoRE MOFs.  $w_j$ ,  $SV_j$ ,  $\rho$ , and  $\beta$  are the SVM model parameters. All these parameters have been given in the first article.<sup>11</sup> After applying the above validity domain constraints, 4269 MOF candidates were remained. For these MOFs, their PE and PA adsorption uptakes at 0.01 and 2 atm were predicted using the ANN models in Equation (8). The detailed model descriptions and parameters have been given in Step 1.<sup>11</sup>

$$q_E = ANN_1(y_1, \dots, y_{19}, P) \text{ at } T = 300\text{K} \quad (8a)$$

$$q_A = ANN_2(y_1, \dots, y_{19}, P) \text{ at } T = 300\text{K} \quad (8b)$$

With the predicted uptakes, the process feasibility constraints in Equation 4–5 were tested for all the 4269 MOFs. As shown in Figure 5, only 364 MOFs are left and considered as feasible for further studies. These 364 MOFs and their corresponding descriptors are tabulated in Supporting Information.

#### 4.2.3 | MOF screening via GCMC simulations

Considering the error of ANN models, the single-component PE and PA adsorption loadings at two pressure levels (0.01 and 2 atm) and 300 K were predicted with rigorous GCMC simulations for the remaining 364 MOFs. The open-source software *RASPA* was employed for this computation.<sup>34</sup> The detailed GCMC settings are described in the Appendix and the computed results are given in Supporting Information. Based on the predicted loadings, it is found that only six MOFs can meet the two feasibility constraints in Equations (4) and (5). In this case, these six MOFs were sent to P/VSA process optimization for quantifying their practical process performance. To do this, GCMC simulations were carried out to calculate the adsorption loadings of PE and PA at five different pressure levels (i.e., 0.01, 0.1, 1, 2, and 5 atm) and 300 K. The results were used to fit the DSL isotherm models in Equation (2) for process optimization. Again, for the six MOFs, their complete GCMC results are provided in Supporting Information.



#### 4.2.4 | MOF screening via P/VSA process optimization

After fitting the eight DSL model parameters for the six MOFs, six isothermal P/VSA process optimizations were performed. It is found that

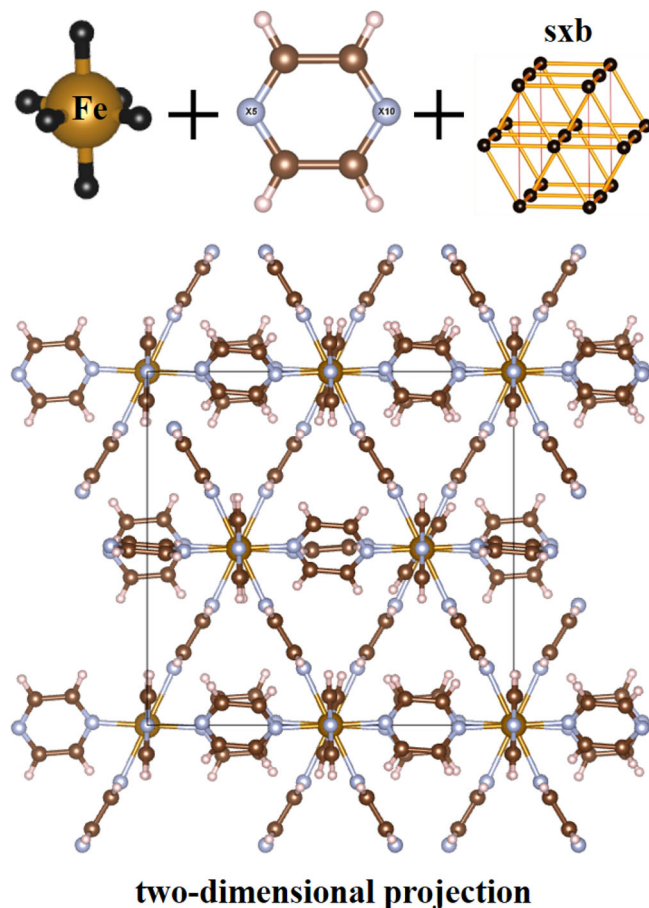


**FIGURE 6** Computationally synthesized optimal metal-organic framework (MOF) for PE/PA separation (visualized by VESTA software)

three of the six candidates can meet the 99% purity and 30% recovery requirements (see also Figure 5). These three computationally synthesized MOFs are named as *SMOF-1*, *SMOF-2*, and *SMOF-3*. Figure 6 shows the building blocks of *SMOF-1* and the corresponding projection to the X-Y plane, and Table S5 lists the crystallographic information file (*cif*) of this MOF. As indicated, *SMOF-1* consists of 6-coordinated iron (Fe) metal node and pyrazine ( $C_4H_4N_2$ ) organic linker assembled in the *sxb* topology. The metal node and organic linker are extracted from CoRE MOF *LEMNOH* and *FUDQIF*, respectively. The other two *SMOFs* are illustrated in Figure S2. Both of them are assembled with an *lcy* topology. *SMOF-2* comprises of 6-coordinated cadmium (Cd) metal and N=N linker. *SMOF-3* owns 6-coordinated iron (Fe) metal connected with C≡N linkers. For the three candidates, their fitted DSL model parameters and corresponding minimum energy consumptions are listed in Table 3. Compared with the benchmark MOF *SEYDUW* (i.e., the best CoRE MOF, see Table 1), *SMOF-1* can achieve a lower energy consumption (72.43 vs. 91.99 kWh/ton PE). In this case, only the results led by *SMOF-1* is discussed below.

#### 4.3 | Optimal results of SMOF-1

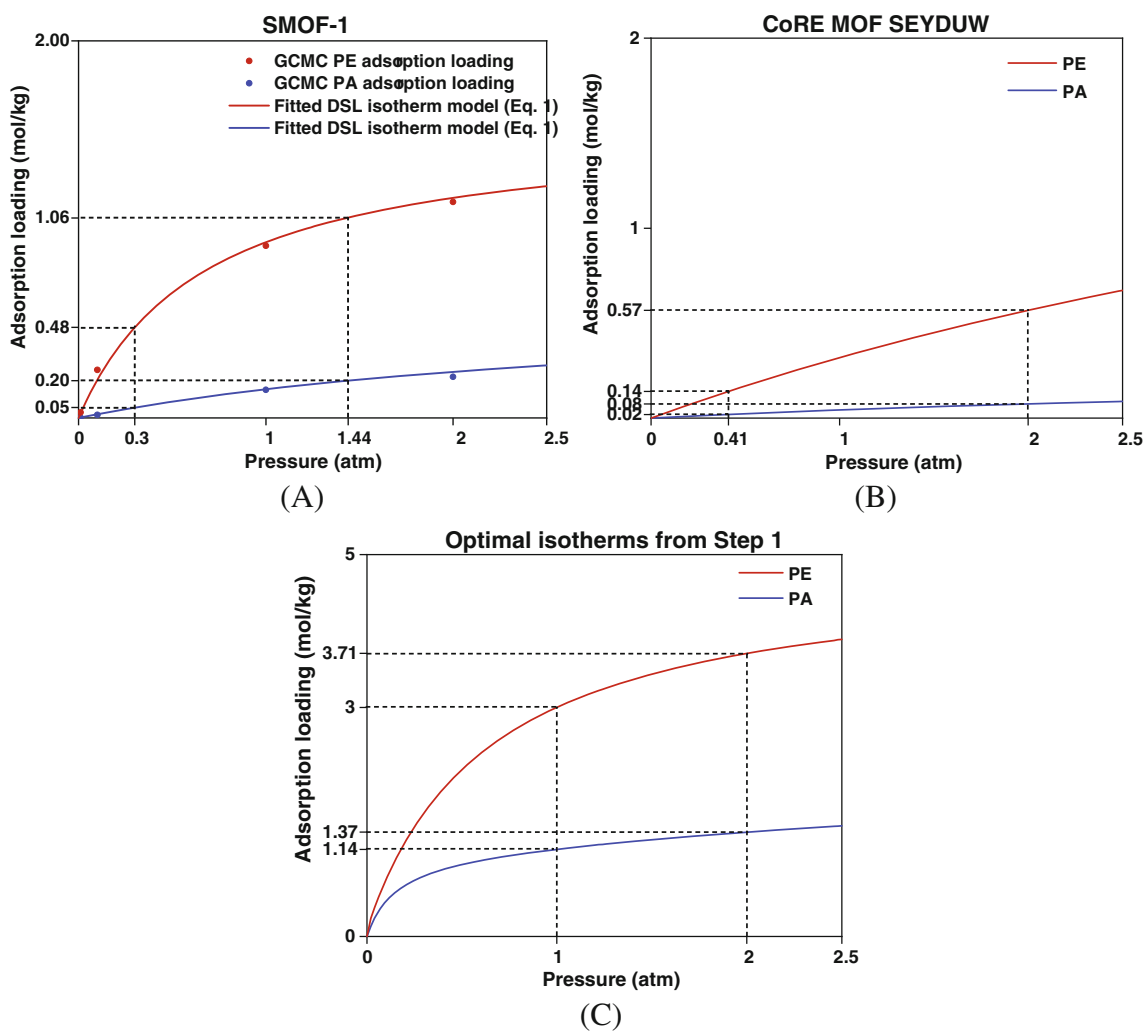
For *SMOF-1*, the optimal P/VSA process operating conditions are listed in the second column of Table 4. The adsorption is performed at 1.44 atm that is lower than the initial pressure 2 atm of the feed gas but higher than the atmospheric pressure. Thus, no gas compression is needed at the pressurization and adsorption steps. Desorption occurs in a vacuum condition of 0.3 atm. Energy is consumed for gas evacuation during desorption and for gas compression at the rinsing step. Comparing the results of *SMOF-1* with *SEYDUW*, it is found that their operating pressures are very different. For *SEYDUW*, the high and low pressures are 2 and 0.41 atm, respectively. The energy consumed at the rinsing step is 46.15 kWh/ton PE that is much larger than that of *SMOF-1* (24.68 kWh/ton PE). This is because *SMOF-1* has a smaller gap between the high and low pressures and hence less energy is needed to re-compress the gases during rinsing.

**TABLE 3** Fitted dual-site Langmuir (DSL) isotherm parameters and the minimum energy consumption for the three synthesized hypothetical metal-organic frameworks (MOFs)

Synthesized MOFs		SMOF-1	SMOF-2	SMOF-3
DSL model parameters	$Q_E^1$	0.4	0.01	2.56
	$b_E^1$	1.48	69.66	0.17
	$Q_E^2$	1.16	4.14	3.35
	$b_E^2$	1.48	0.1	0.12
	$Q_A^1$	0.06	0.65	1.03
	$b_A^1$	2.3	0.12	0.13
	$Q_A^2$	1.09	0.65	1.19
	$b_A^2$	0.1	0.12	0.13
Energy consumption (kWh/ton PE)		72.43	118.82	303.94

**TABLE 4** Optimization results of four-step isothermal pressure/vacuum swing adsorption (P/VSA) process with three different metal-organic frameworks (MOFs)

	Process using SMOF-1	Process using SEYDUW	Optimal process from step 1 <sup>11</sup>
PR duration (s)	12.2	30	13.0
AD duration (s)	30.3	10.1	22.1
RI duration (s)	6.4	5.0	5.6
DE duration (s)	600	600	600
High pressure (atm)	1.44	2	2
Low pressure (atm)	0.3	0.41	1
PE purity	0.99	0.99	0.99
PE recovery	0.30	0.30	0.30
PE production rate (mol/h)	203.6	117.8	210.6
Initial selectivity at high pressure	10.1	7.2	33.9
Energy consumption at pressurization (kWh/ton PE)	0	0	0
Energy consumption at adsorption (kWh/ton PE)	0	0	0
Energy consumption at rinsing (kWh/ton PE)	24.68	46.15	12.8
Energy consumption at desorption (kWh/ton PE)	47.75	45.84	0
Total energy consumption (kWh/ton PE)	72.43	91.99	12.8

**FIGURE 7** Single-component adsorption isotherms for (A) SMOF-1, (B) SEYDUW, and (C) optimal hMOF from Step 1

In fact, the root reasons for different results can be explained by their different adsorption isotherms. As shown in Figure 7, *SMOF-1* exhibits a larger gap of PE and PA isotherms than *SEYDUW*. With the DSL parameters in Table 3, the initial selectivity of *SMOF-1* at the adsorption condition is calculated to be 10.1, larger than that of *SEYDUW*. This helps producing high-purity PE product. In addition, *SMOF-1* provides a better condition for adsorption and desorption. Its PE loading difference between 1.44 and 0.3 atm already reaches 0.58 mol/kg, which helps achieving the required 30% PE recovery. By contrast, for *SEYDUW*, a large pressure drop between adsorption and desorption (i.e., from 2 to 0.41 atm) is needed to ensure that enough PE is adsorbed and recovered. This directly leads to a higher energy consumption at the rinsing step. The forth column of Table 4 lists the optimal process target obtained from Step 1 and Figure 7C shows its corresponding optimal isotherms.<sup>11</sup> Clearly, the process performance led by *SMOF-1* is worse than that of the optimal process target. In other words, there are still substantial spaces for finding new MOFs whose isotherms can be closer to the optimal isotherm target.

## 5 | CONCLUSION

This article presents the second step of our novel framework for the integrated MOF and P/VSA process design, that is, the matching of optimal MOF descriptors by existing MOF material structures. Multiple open-source computational tools and in-house programs have been used for *in silico* MOF synthesis and screening. First, based on the optimal isotherm targets obtained from Step 1, the explicit relationships between adsorption properties and process feasibility were identified to develop model-based constraints for fast preliminary MOF screening. Afterward, MOF building blocks were generated from 471 MOFs in the CoRE MOF database and used to create new hypothetical MOFs. The created MOF candidates were screened using the developed model-based constraints. In addition, GCMC simulations and P/VSA process optimization were performed to further screen the MOFs. As a result, the best MOF candidate was identified, which shows a much better PE/PA separation performance than the benchmark MOF *SEYDUW*.

To the best of our knowledge, this is the first attempt in the process systems engineering community to perform a computer-aided design of solid adsorbent materials. The major novelty of the present work is the incorporation of insights from the phase and process levels for efficient MOF design on the basis of a multi-scale design framework. The optimal MOF found can better serve the P/VSA-based separation process and improves separation efficiency significantly. Despite the large progress achieved, there are still some limitations. First, only a fixed cycle configuration is considered. In fact, the synthesis of optimal P/VSA processes can provide additional benefits for enhancing the separation efficiency, in particular when material design is integrated.<sup>35</sup> Given the huge complexity of the integrated material and process synthesis problem, using short-cut or surrogate process models can be a promising solution strategy. Second, since only certain known rules regarding the building block compatibility are

accounted for in *ToBaCCo*, the hypothetical MOFs created can be nonexistent or difficult to synthesize from the experimental perspective. Thus, additional constraints on MOF stability (e.g., chemical,<sup>36</sup> mechanical,<sup>37</sup> and thermal<sup>38,39</sup>) and synthesizability<sup>40</sup> will be worth adding into future screening procedures. Moreover, structural optimization should be carried out to rectify the bond lengths and angles of the MOFs for further improving the reliability. Efforts will be made in these directions in our next research activities.

## AUTHOR CONTRIBUTIONS

**Xiang Zhang:** Investigation (lead); methodology (lead); software (lead); writing – original draft (lead). **Teng Zhou:** Funding acquisition (equal); project administration (lead); supervision (lead); writing – review and editing (lead). **Kai Sundmacher:** Conceptualization (lead); funding acquisition (lead); resources (lead); writing – review and editing (equal).

## ACKNOWLEDGMENTS

Xiang Zhang acknowledges the financial support of this work by the Max Planck Institute for Dynamics of Complex Technical Systems in Magdeburg, Germany, via the Ernst Dieter Gilles Postdoctoral Fellowship. Teng Zhou acknowledges the financial support from the Max Planck Society, Germany, for his Junior Professorship at OvGU Magdeburg on Computer-Aided Material and Process Design (CAMPD). Kai Sundmacher acknowledges the support from the EU-program ERDF (European Regional Development Fund) of the German Federal State Saxony-Anhalt within the Research Center of Dynamic Systems (CDS).

Open Access funding enabled and organized by Projekt DEAL.

## DATA AVAILABILITY STATEMENT

The data that support the findings of this study are available from the corresponding author upon reasonable request.

## ORCID

Teng Zhou  <https://orcid.org/0000-0003-1941-5348>

Kai Sundmacher  <https://orcid.org/0000-0003-3251-0593>

## REFERENCES

1. Daglar H, Keskin S. Recent advances, opportunities, and challenges in high-throughput computational screening of MOFs for gas separations. *Coord Chem Rev.* 2020;422:213470.
2. First EL, Hasan MMF, Floudas CA. Discovery of novel zeolites for natural gas purification through combined material screening and process optimization. *AIChE J.* 2014;60(5):1767-1785.
3. Sun W, Lin L-C, Peng X, Smit B. Computational screening of porous metal-organic frameworks and zeolites for the removal of SO<sub>2</sub> and NO<sub>x</sub> from flue gases. *AIChE J.* 2014;60(6):2314-2323.
4. Farmahini AH, Krishnamurthy S, Friedrich D, Brandani S, Sarkisov L. Performance-based screening of porous materials for carbon capture. *Chem Rev.* 2021;121(17):10666-10741.
5. Findley JM, Sholl DS. Computational screening of MOFs and zeolites for direct air capture of carbon dioxide under humid conditions. *J Phys Chem C.* 2021;125(44):24630-24639.
6. Uebbing J, Biegler LT, Rihko-Struckmann L, Sager S, Sundmacher K. Optimization of pressure swing adsorption via a trust-region filter algorithm and equilibrium theory. *Comput Chem Eng.* 2021;151:107340.

7. Agarwal A, Biegler LT, Zitney SE. Simulation and optimization of pressure swing adsorption systems using reduced-order modeling. *Ind Eng Chem Res.* 2009;48(5):2327-2343.
8. Subraveti SG, Li Z, Prasad V, Rajendran A. Machine learning-based multiobjective optimization of pressure swing adsorption. *Ind Eng Chem Res.* 2019;58(44):20412-20422.
9. Pullumbi P, Brandani F, Brandani S. Gas separation by adsorption: technological drivers and opportunities for improvement. *Curr Opin Chem Eng.* 2019;24:131-142.
10. Sen T, Kawajiri Y, Realf MJ. Integration of material and process design for kinetic adsorption separation. *Ind Eng Chem Res.* 2021;60(6):2536-2546.
11. Zhang X, Zhou T, Sundmacher K. Integrated metal-organic framework and pressure/vacuum swing adsorption process design: descriptor optimization. *AIChE J.* 2021;68(2):e17524.
12. Khurana M, Farooq S. Integrated adsorbent-process optimization for carbon capture and concentration using vacuum swing adsorption cycles. *AIChE J.* 2017;63(7):2987-2995.
13. Khurana M, Farooq S. Integrated adsorbent process optimization for minimum cost of electricity including carbon capture by a VSA process. *AIChE J.* 2019;65(1):184-195.
14. Rosen AS, Notestein JM, Snurr RQ. Realizing the data-driven, computational discovery of metal-organic framework catalysts. *Curr Opin Chem Eng.* 2022;35:100760.
15. Altintas C, Altundal OF, Keskin S, Yildirim R. Machine learning meets with metal organic frameworks for gas storage and separation. *J Chem Inf Model.* 2021;61(5):2131-2146.
16. Wilmer CE, Leaf M, Lee CY, et al. Large-scale screening of hypothetical metal-organic frameworks. *Nat Chem.* 2012;4(2):83-89.
17. Bao Y, Martin RL, Simon CM, Haranczyk M, Smit B, Deem MW. In silico discovery of high deliverable capacity metal-organic frameworks. *J Phys Chem C.* 2015;119(1):186-195.
18. Lee S, Kim B, Cho H, et al. Computational screening of trillions of metal-organic frameworks for high-performance methane storage. *ACS Appl Mater Interfaces.* 2021;13(20):23647-23654.
19. Lan Y, Han X, Tong M, et al. Materials genomics methods for high-throughput construction of COFs and targeted synthesis. *Nat Commun.* 2018;9(1):5274.
20. Yao Z, Sánchez-Lengeling B, Bobbitt NS, et al. Inverse design of nanoporous crystalline reticular materials with deep generative models. *Nat Mach Intell.* 2021;3(1):76-86.
21. Majumdar S, Moosavi SM, Jablonka KM, Ongari D, Smit B. Diversifying databases of metal organic frameworks for high-throughput computational screening. *ACS Appl Mater Interfaces.* 2021;13(51):61004-61014.
22. Zhang X, Zhang K, Yoo H, Lee Y. Machine learning-driven discovery of metal-organic frameworks for efficient CO<sub>2</sub> capture in humid condition. *ACS Sustainable Chem Eng.* 2021;9(7):2872-2879.
23. Lim Y, Park J, Lee S, Kim J. Finely tuned inverse design of metal-organic frameworks with user-desired Xe/Kr selectivity. *J Mater Chem A.* 2021;9(37):21175-21183.
24. Rajagopalan AK, Avila AM, Rajendran A. Do adsorbent screening metrics predict process performance? A process optimisation based study for post-combustion capture of CO<sub>2</sub>. *Int J Greenh Gas Control.* 2016;46:76-85.
25. Khurana M, Farooq S. Adsorbent screening for postcombustion CO<sub>2</sub> capture: a method relating equilibrium isotherm characteristics to an optimum vacuum swing adsorption process performance. *Ind Eng Chem Res.* 2016;55(8):2447-2460.
26. Ga S, Jang H, Lee JH. New performance indicators for adsorbent evaluation derived from a reduced order model of an idealized PSA process for CO<sub>2</sub> capture. *Comput Chem Eng.* 2017;102:188-212.
27. Tang D, Wu Y, Verploegh RJ, Sholl DS. Efficiently exploring adsorption space to identify privileged adsorbents for chemical separations of a diverse set of molecules. *ChemSusChem.* 2018;11(9):1567-1575.
28. Iyer SS, Hasan MMF. Mapping the material-property space for feasible process operation: application to combined natural-gas separation and storage. *Ind Eng Chem Res.* 2019;58(24):10455-10465.
29. Tang S-F, Song J-L, Li X-L, Mao J-G. Luminescent lanthanide(III) carboxylate-phosphonates with helical tunnels. *Cryst Growth des.* 2006;6(10):2322-2326.
30. Colón YJ, Gómez-Gualdrón DA, Snurr RQ. Topologically guided, automated construction of metal-organic frameworks and their evaluation for energy-related applications. *Cryst Growth des.* 2017;17(11):5801-5810.
31. Anderson R, Gómez-Gualdrón DA. Increasing topological diversity during computational "synthesis" of porous crystals: how and why. *CrstEngComm.* 2019;21(10):1653-1665.
32. O'Boyle NM, Banck M, James CA, Morley C, Vandermeersch T, Hutchison GR. Open babel: an open chemical toolbox. *J Chem.* 2011;3(1):33.
33. Sarkisov L, Bueno-Perez R, Sutharson M, Fairen-Jimenez D. Materials informatics with PoreBlazer v4.0 and the CSD MOF database. *Chem Mater.* 2020;32(23):9849-9867.
34. Dubbeldam D, Calero S, Ellis DE, Snurr RQ. RASPA: molecular simulation software for adsorption and diffusion in flexible nanoporous materials. *Mol Simul.* 2016;42(2):81-101.
35. Dowling AW, Vetukuri SRR, Biegler LT. Large-scale optimization strategies for pressure swing adsorption cycle synthesis. *AIChE J.* 2012;58(12):3777-3791.
36. Batra R, Chen C, Evans TG, Walton KS, Ramprasad R. Prediction of water stability of metal-organic frameworks using machine learning. *Nat Mach Intell.* 2020;2(11):704-710.
37. Moghadam PZ, Rogge SMJ, Li A, et al. Structure-mechanical stability relations of metal-organic frameworks via machine learning. *Matter.* 2019;1(1):219-234.
38. Nandy A, Duan C, Kulik HJ. Using machine learning and data mining to leverage community knowledge for the engineering of stable metal-organic frameworks. *J Am Chem Soc.* 2021;143(42):17535-17547.
39. Gee JA, Sholl DS. Characterization of the thermodynamic stability of solvated metal-organic framework polymorphs using molecular simulations. *J Phys Chem C.* 2013;117(40):20636-20642.
40. Anderson R, Gómez-Gualdrón DA. Large-scale free energy calculations on a computational metal-organic frameworks database: toward synthetic likelihood predictions. *Chem Mater.* 2020;32(19):8106-8119.

## SUPPORTING INFORMATION

Additional supporting information may be found in the online version of the article at the publisher's website.

**How to cite this article:** Zhang X, Zhou T, Sundmacher K. Integrated metal-organic framework (MOF) and pressure/vacuum swing adsorption process design: MOF matching. *AIChE J.* 2022;68(9):e17788. doi:10.1002/aic.17788

## APPENDIX

### GCMC SIMULATIONS

In the GCMC simulation, all the MOFs were assumed to be rigid while propane and propene were regarded as flexible molecules including intramolecular interactions for bonds, angles, and torsions. To obtain statistically good results,  $10^5$  Monte Carlo cycles were simulated including  $5 \times 10^4$  initialization cycles and  $5 \times 10^4$  equilibrium cycles. Each cycle includes four possible motions (translation, rotation, reinsertion, and swap) with equal probability. The fugacity coefficient was simply set to 1, since only moderate operating pressures were considered. The Ewald summation method was applied to calculate electrostatic interactions with a relative precision of  $10^{-6}$ . Force field parameters are required to compute interactions of adsorbate-

adsorbent and adsorbate-adsorbate pairs. As widely accepted, the interaction energies were computed through the Lennard-Jones (LJ) potentials. The LJ parameters for the adsorbent atoms were taken from the Universal Force Field (UFF). The adsorbates propane and propene were considered as combinations of  $\text{CH}_3$ ,  $\text{CH}_2$ , and  $\text{CH}$ . Their associated LJ parameters were taken from the standard TraPPE-UA force field. It has been widely reported that the use of UFF for MOFs and TraPPE-UA for hydrocarbons can produce reasonable adsorption results. In addition, the Lorentz-Berthelot mixing rule was chosen as the adsorbate-adsorbent interaction method and the cutoff distance was defined as 12 Å. In order to validate the reliability of our GCMC simulations, the adsorptions of propane and propene in ZIF-8 at 293 K and 0–1 bar were simulated. Figure S3 shows that the predicted isotherms match closely with the experimental ones.